JACS
JOURNAL OF THE AMERICAN CHEMICAL SOCIETY
Article
pubs.acs.org/JACS

DNA Origami Based Visualization System for Studying Site-Specific Recombination Events

Yuki Suzuki,[†,§] Masayuki Endo,*[,‡,§] Yousuke Katsuda,[†] Keiyu Ou,[†] Kumi Hidaka,[‡] and Hiroshi Sugiyama*[,†,‡,§]

[†]Department of Chemistry, Graduate School of Science, Kyoto University, Kitashirakawa-oiwakecho, Sakyo-ku, Kyoto 606-8502, Japan

[‡]Institute for Integrated Cell-Material Sciences (WPI-iCeMS), Kyoto University, Yoshida-ushinomiyacho, Sakyo-ku, Kyoto 606-8501, Japan

[§]CREST, Japan Science and Technology Corporation (JST), Sanbancho, Chiyoda-ku, Tokyo 102-0075, Japan

Supporting Information

ABSTRACT: Site-specific recombination involves reciprocal exchange between defined DNA sites. The reaction initiates from the formation of a recombinase–DNA synaptic complex, in which two recombination sites arrange in an appropriate configuration. However, there is incomplete information about how the topological state of the substrate influences the synapsis and outcome of the reaction. Here, we show that Cre-mediated recombination can be regulated by controlling the orientation and topology of the *loxP* substrate in a DNA frame nanoscaffold. High-speed atomic force microscopy analyses revealed that the *loxP*-containing substrate strands in the antiparallel orientation can be recombined only through formation of synaptic complexes. By tethering Holliday junction (HJ) intermediates to DNA frames in different connection patterns and using them as a starting substrate, we found that the topological state of the HJ intermediates dictates the outcome of the resolution. Our approach should provide a new platform for structural–functional studies of various DNA targeting enzymes, especially which require formation of synaptic complexes.

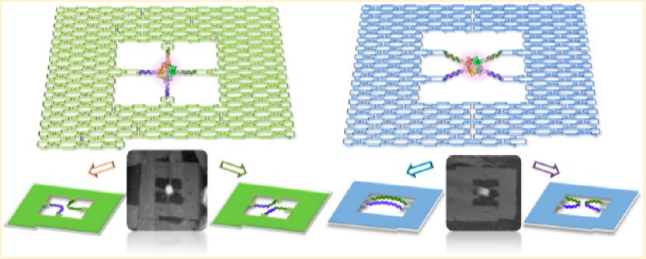

INTRODUCTION

Site-specific recombination, which brings about genetic rearrangement in processes such as DNA integration, excision, and inversion, involves strand exchange between segments having a limited extent of sequence homology. *Escherichia coli* phage P1 Cre recombinase catalyzes site-specific recombination between two 34-base pair (bp) *loxP* sites (Figure 1).[1] The Cre-mediated reaction starts from the formation of a synaptic complex. Two monomers bind to half of an inverted repeat sequence,[2,3] and two of these complexes (presynaptic complexes) form one synaptic tetramer complex via protein–protein interactions.[4,5] The two *loxP* sites are arranged in antiparallel fashion when in the Cre–*loxP* synaptic complex.[6] Among the four monomers, only two are active at any time. Thus, the recombination is achieved by stepwise strand exchange, during which one pair of DNA strands is first exchanged between recombining sites to form a four-way Holliday junction (HJ) intermediate, and the second pair of strands is then exchanged upon the resolution of the HJ, thus generating the resulting recombinant products.[7] Importantly, Cre catalyzes the reaction without the need for other accessary proteins or high-energy cofactors.[4] The minimum requirement of the Cre recombination system and its ability to function in eukaryotic cells have led to its widespread use as a genome engineering tool for both *in vitro* and *in vivo* DNA manipulations.[7−10]

The recombination process mediated by Cre–*loxP* has been studied using various experimental approaches[6,11−13] including single-molecule techniques.[14−16] Recent studies based on tethered particle motion (TPM) have revealed the kinetics of each elementary step in the recombination reactions from beginning to end.[15] Further details of the reaction and the kinetics of strand rearrangement within individual complexes have since been provided by tethered fluorophore motion (TFM) analysis.[16] Although these techniques allow the recombination to be detected by monitoring the changes in the Brownian motion of the tethered beads or in the fluorescent signals, regulation of the relative orientation of two substrate *loxP* sites has not been achieved, because detection of the complex formation in those approaches relies on the large-scale DNA motions.

In the current study, we used a frame-like DNA origami scaffold (DNA frame)[17−22] in which two *loxP* site-containing double-stranded DNAs (dsDNAs) can be arranged in parallel or antiparallel orientations. Because both ends of the strands

Received: August 21, 2013
Published: December 12, 2013

   dx.doi.org/10.1021/ja408656y | J. Am. Chem. Soc. 2014, 136, 211−218

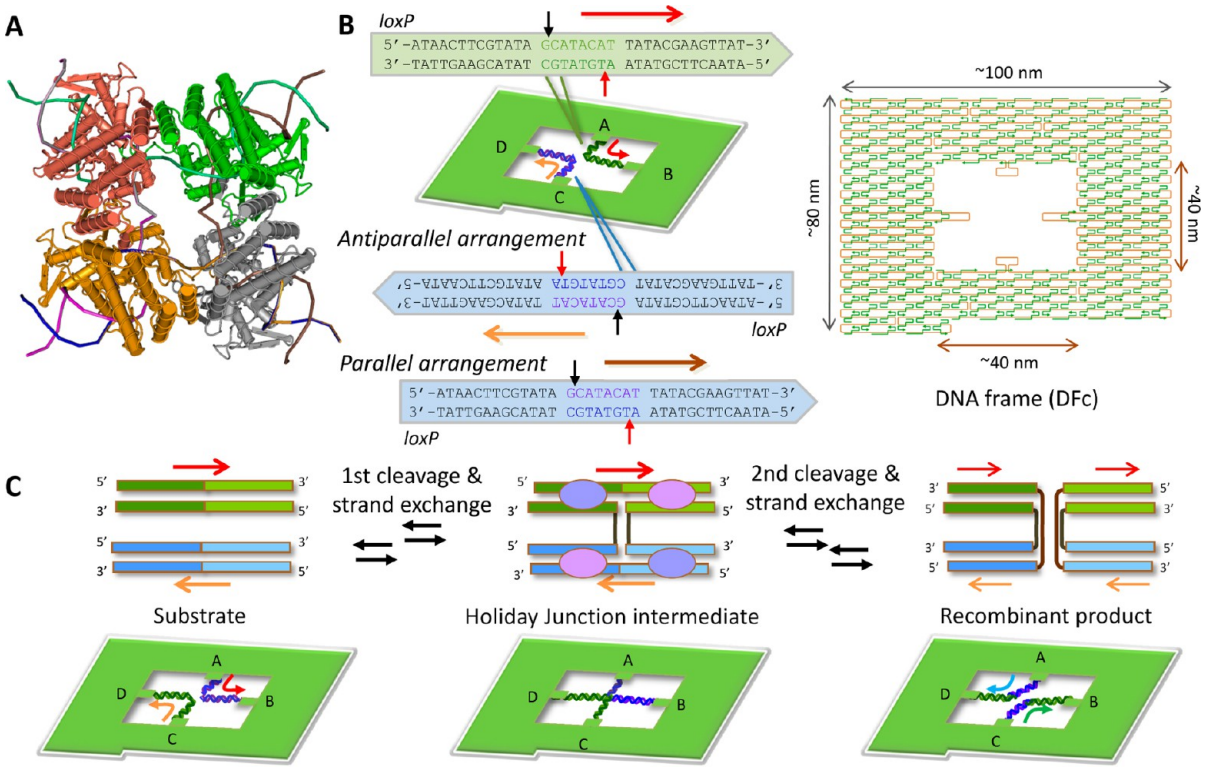

Figure 1. DNA frame structure for the incorporation of *loxP* site-containing DNAs. (A) Crystal structure of Cre tetramer bound to HJ intermediate (PDB: 3CRX). (B) A designed DNA origami scaffold (DNA frame with two pairs of perpendicular connectors: DFc). DFc carrying two dsDNAs and the sequences of the *loxP* site at the center of the strands. Two different orientations of *loxP* sites were achieved by changing the strand connected between C−D. Black and red arrows indicate positions of G↓C cleavage and A↓T cleavage, respectively. (C) Schematic of Cre−*loxP* site-specific recombination pathway and corresponding configuration of the bridged strands in the DFc at each step.

are tethered to the DNA frame, the recombination products are clearly distinguishable from the substrates by viewing the connection patterns of the two duplex strands in the DNA frame. By combining this system with high-speed atomic force microscopy (HS-AFM) imaging, we directly monitored the Cre-mediated site-specific recombination process at a single-molecule level in the context of the substrate *loxP* site orientation that influences the synapsis and the subsequent reaction. We also analyzed the cleavage order in the recombination by starting the reaction from a *loxP*-derived antiparallel HJ. Controlled incorporation of four DNA arms of the HJ at various angles was achieved using two different designs of DNA frame nanostructures. The results of the resolution of the HJs in two different DNA frames offer strong evidence of the effect of the topological state of the junction, which affects the cleavage preference and direction of the subsequent resolution.

RESULTS

DNA Frame Formation and Incorporation of Two *loxP* Site-Containing dsDNAs. The DNA origami nanoscaffold (DNA frame) has a vacant rectangular area inside, in which two pairs of perpendicular connectors were introduced for hybridization of the two different *loxP*-containing dsDNAs (Figure 1B); for convenience, we call this DNA frame "DFc". The DFc was formed using M13mp18 single-stranded DNA and sequence-designed DNA strands (staple strands) in buffer containing 20 mM Tris-HCl (pH 7.6), 1 mM EDTA, and 10 mM $MgCl_2$. The DNA components were annealed by decreasing the temperature from 85 to 15 °C at a rate of −1.0 °C/min. AFM images of the DFc structure revealed accurate formation of the predesigned shape, which had the four connection points and the orientation marker (Figure S1).

Two *loxP*-containing DNA strands were introduced into the preassembled DFc through selective hybridization between the connection sites A−B and C−D (Figure 1B). By changing the orientation of the strand between the C−D sites, two *loxP* sites could be arranged in parallel/antiparallel in the DFc. The assembly was performed in a buffer containing 20 mM Tris-HCl (pH 7.6), 1 mM EDTA, and 10 mM $MgCl_2$ by annealing the mixture from 40 to 15 °C at a rate of −1.0 °C/min. The assembled structure was imaged by AFM in the same buffer condition. Visualization revealed that the two incorporated DNA strands were separated clearly in the DFc, demonstrating that the duplexes are long enough to fit into the connection sites but short enough to prevent overlapping of the two strands (Figure 2A). The incorporation of the pair of duplex worked with high yield over 90% (92%, N = 146) (Figure S2). Time-lapse HS-AFM imaging of the DFc with the two duplex strands showed the flexible feature of the strands (Figure 2B). The distances between the two strands measured from the section profile (Figure S2) are plotted in Figure 2C. Upward and downward changes in the distance indicate that both strands are flexible enough to allow changes in the duplex structures in the DFc. We note that the DNA frame was stably absorbed onto the mica surface, whereas the DNAs inside were sufficiently mobile on the surface. This allowed us to monitor the dynamic processes of the recombination reaction.

Reaction with Antiparallel *loxP* Substrates. Because the structural studies of the Cre−*loxP* synaptic complex revealed

dx.doi.org/10.1021/ja408656y | J. Am. Chem. Soc. 2014, 136, 211−218

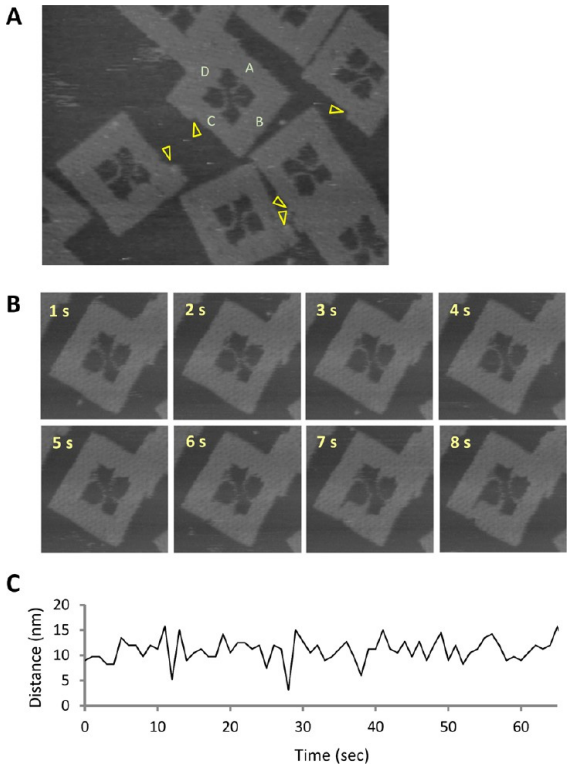

Figure 2. AFM analyses of DFc carrying two dsDNAs. (A) AFM image of DFc carrying two *loxP* site-containing DNAs in antiparallel orientation (DFc–$loxP_{ap}$). Image size: 400 × 300 nm. Four connection points can be identified by the orientation marker (yellow triangle). (B) Successive HS-AFM images of DFc–$loxP_{ap}$ obtained at 1.0 frame per second (fps). The elapsed time is shown in each image. Image size: 180 × 180 nm. (C) Trajectory of distance between two DNA strands. Peak-to-peak distances (red triangles in Figure S2) in each time point were measured. Details are seen in Movie S1.

four Cre monomers bound to two antiparallel *loxP* sites, we first examined the Cre-mediated recombination reaction with DFc in which two *loxP* sites were arranged in an antiparallel orientation (DFc–$loxP_{ap}$). Figure 3A shows a representative static AFM image of DFc–$loxP_{ap}$ obtained after the 30 min reaction with Cre recombinase. In addition to the substrate structure, the DFc–$loxP_{ap}$ having a clear-cut X-shape morphology with a bright spot at the center comprised around 23% of the frame and was attributed to Cre–*loxP* synaptic complex formation. DFc–$loxP_{ap}$, whose DNA strands were connected between sites A–D and B–C, was observed (Figures 3B and S3) and corresponded to the recombinants (Figure 1C). These results demonstrate that the two *loxP* sites in DFc can be close enough to allow Cre-mediated synapsis and site-specific recombination.

To confirm the Cre–*loxP* recombination in DFc, time-course analysis was performed by AFM. Micrographs were taken of the reaction mixture containing DFc–$loxP_{ap}$ and Cre after 7.5, 15, 30, 60, 120, and 240 min at 37 °C. Quantitative data are shown in Figure 3C. Recombination was already advanced within 7.5 min, and a number of recombinants were observed together with the synaptic complexes after 30 min. The appearance frequencies of the recombinants reached a plateau 60 min after mixing. The yield of recombinant was relatively lower than those reported by bulk experiments, probably due to the limited flexibility of the framed substrates. It is noteworthy that presynaptic complexes, in which a single *loxP* site was occupied with the Cre dimer (Figure S4), were observed rarely (Table S1). This indicates that these intermediate complexes have a short lifetime and that the Cre molecules dissociate quickly after the release of the recombinants.

To gain further understanding about how the recombinants are generated, the conversion of the Cre–*loxP* synaptic complex to recombinants was monitored directly by HS-AFM imaging. Figure 3D shows a series of time-lapse images of synaptic complexes formed with two *loxP* sites in antiparallel orientation in the DFc that produced recombinants followed by the dissociation of the Cre. The Cre tetramer was observed to bind the two *loxP* sites, thus forming the synaptic complex. This complex remained until 4 s. The brightness (height) of the protein spot decreased at 5 s, indicating destabilization of the Cre–Cre or Cre–*loxP* interactions. At 6 s, the protein was seen to split into four monomer particles, which dissociated from the sites, leaving recombinant strands. This is consistent with the knowledge that the Cre tetramer is formed only when bound to two *loxP* sites but exists as a monomer when free in solution.

Reaction with Parallel *loxP* Substrates. We next examined the reaction with DFc in which two *loxP* sites containing DNA were arranged in parallel orientation (DFc–$loxP_p$). AFM images of DFc–$loxP_p$ obtained after the reaction with Cre recombinase also revealed Cre binding at the center of the two substrate strands (Figures 4A and S5), indicating that two *loxP* sites can be synapsed upon binding of Cre even if they are arranged in parallel.

The statistical analysis of the time-course data showed an increase in the synaptic complex population but no increase in the recombinant population (cross-shaped structure) (Figures 4B and S6). This result indicates that the Cre tetramer bound to two parallel *loxP* site-containing strands is incapable of achieving recombination. Thus, its dissociation would result solely in the release of the substrate strands.

Time-lapse HS-AFM imaging of the individual Cre–$loxP_p$ complex showed the dissociation process of the Cre tetramer (Figure 4C). A bright spot characteristic of the complex was seen clearly until 5 s. At 6 s, the brightness of the complex decreased, suggesting destabilization of the complex. In the image at 7 s, each *loxP* site was seen to be bound to the split particle, probably the Cre dimer. At 8 s, the protein dissociated into four monomers, leaving two separate dsDNAs, whose connection pattern in the DFc was the same as in the substrate structure.

Preferential Cleavage of *loxP*-Derived HJ Intermediates. Despite the highly symmetric nature of the Cre–*loxP* system, there is strong evidence that Cre exchanges *loxP* strands in specific order by cleaving at the G↓C sites first rather than the A↓T sites[23−25] (Figure 5A). It has also been shown that, when the reaction is started with HJ intermediates, Cre preferentially resolves them by A↓T cleavage.[26] However, these indications are mainly from studies with mutated Cre or modified *loxP*, and there are conflicting conclusions about which order is preferred.[27,28]

To address the issue of the cleavage preference, we introduced the antiparallel HJ intermediates into DFc with two different connection patterns (Figures 5B and S7). $loxP_{ap}$HJ-a had A↓T sites between the connection sites B–C and D–A, whereas $loxP_{ap}$HJ-b had A↓T sites between the connection sites A–B and C–D. If A↓T cleavage is preferred, resolution of $loxP_{ap}$HJ-a and $loxP_{ap}$HJ-b in DFc should give connection patterns of type I (DFc where two duplex strands are connected between sites A–B and C–D) and type II (DFc

dx.doi.org/10.1021/ja408656y | J. Am. Chem. Soc. 2014, 136, 211−218

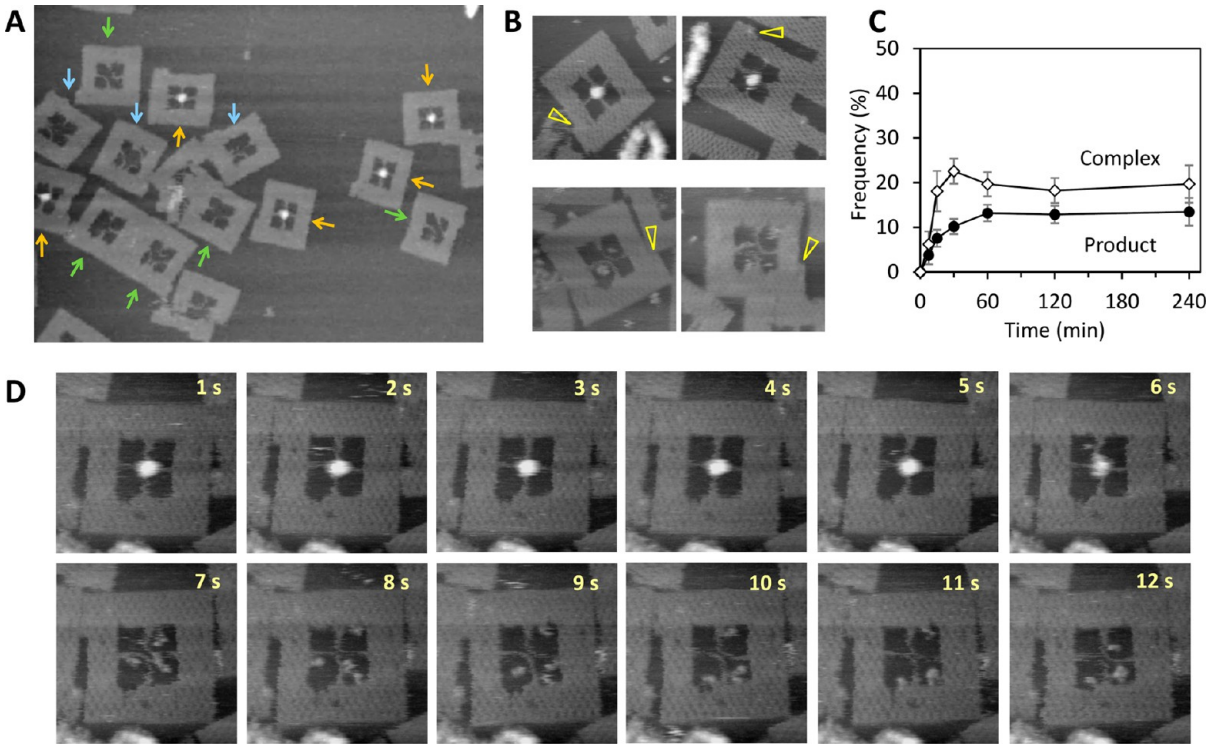

Figure 3. Cre–*loxP* site specific recombination with DFc–*loxP*$_{ap}$. (A) Representative AFM image of DFc–*loxP*$_{ap}$ after the reaction with Cre. Green, orange, and blue arrows indicate substrates, synaptic complexes, and recombinants, respectively. Image size: 800 × 600 nm. (B) Highly magnified AFM images of synaptic complex (top; cross-shape with bound protein) and recombinant (bottom; DFc in which two duplex strands are connected between B–C and D–A). Image size: 180 × 180 nm. (C) Time-course analysis of the appearance of distinct structures; synaptic complex and recombinant. The number of each type of DNA frames observed was counted (total of 250–400 DNA frames analyzed for each time point). Error bars represent the standard deviation based on four different imaging experiments. (D) Successive HS-AFM images of a DFc–*loxP*$_{ap}$–Cre synaptic complex which produced recombination product. Images were obtained at scan rate of 1.0 fps. The elapsed time is shown in each image. Image size: 180 × 180 nm. Details are seen in Movie S2.

where two duplex strands are connected between sites B–C and A–D), respectively. Figure 5C shows a representative AFM image of *loxP*$_{ap}$HJ-a obtained after the 30 min reaction with Cre recombinase (see also Figure S8). Both type I and II configurations can be seen in the image. To characterize the cleavage preference, AFM micrographs were taken for the reaction mixture containing Cre and DFc that had incorporated *loxP*$_{ap}$HJ-a or *loxP*$_{ap}$HJ-b after 15, 30, 60, 120, and 240 min at 37 °C, and changes in the appearance frequencies of type I and type II configurations were plotted (Figure 5D,E). As shown in Figure 5D, reaction of Cre with *loxP*$_{ap}$HJ-a yielded type I product with around a 2-fold preference, suggesting that Cre efficiently resolved *loxP*$_{ap}$HJ-a by A↓T cleavage. Resolution of *loxP*$_{ap}$HJ-b showed a similar bias for the A↓T cleavage, as reflected in the accumulation of the type II product (Figures 5E, S8 and S9). We therefore concluded that Cre preferentially resolves DFc-incorporated HJ intermediates by A↓T cleavage.

Resolution of the *loxP*-Derived HJs in Alternative Configurations. It is thought that the catalytic preferences of Cre can be attributed to a spacer region in the *loxP* site because the spacer region is the only source of asymmetry in the system and it affects the conformation of the HJ intermediates. Given this idea, one may assume that the outcome of the nicking reaction can be affected by the topology of the HJ intermediates.

To verify this hypothesis, we used a previously reported DNA frame (DFp),[17−21] in which two pairs of parallel connecters were introduced to tether the same size of antiparallel HJ (Figure S10). Two different connection patterns of the arms of the HJ were examined (Figures 6A and S10). We reasoned that the nicking reaction should produce two possible structural patterns, namely two separate parallel DNA strands (type I′) or two separate double-looped DNA structures (type II′), depending on the cleavage site (Figure 6A). HS-AFM observations of the Cre-mediated resolution of *loxP*$_{ap}$HJ-a′ demonstrated the production of both type I′ and II′ configurations (Figure S11). Both types of configuration were also seen in the static AFM image of *loxP*$_{ap}$HJ-a′ obtained after the 30 min reaction with Cre recombinase (Figure 6B, see also Figures S12 and S14). As expected from the cleavage preference, the treatment of *loxP*$_{ap}$HJ-a′ with Cre resulted in accumulation of type I′ structure, i.e., product of A↓T cleavage with around a 5-fold preference (Figure 6C). By contrast, the reaction with *loxP*$_{ap}$HJ-b′ did not follow the expected preference. Type I′ structures accumulated preferentially, indicating efficient resolution of *loxP*$_{ap}$HJ-b′ by C↓G cleavage (Figures 6D and S13). This result provides a clear contrast to the preference observed with the DFc-incorporated HJs, in which the product of A↓T cleavage was more efficient in both connection patterns, indicating the critical role of DNA topology in determining the reaction biases.

■ DISCUSSION

We have reported here the construction of orientation-controlled substrate DNA strands and the single-molecule visualization of Cre–*loxP* recombination. Using HS-AFM

dx.doi.org/10.1021/ja408656y | J. Am. Chem. Soc. 2014, 136, 211−218

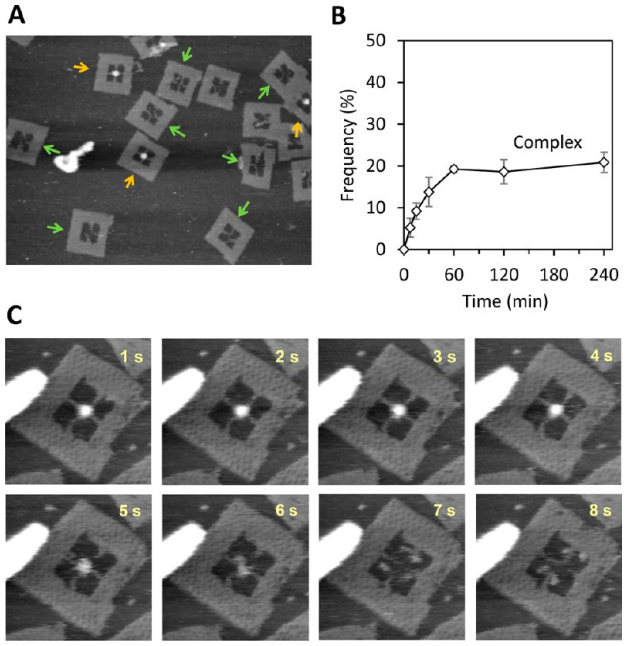

Figure 4. Cre binding to DFc–$loxP_p$. (A) Representative AFM image of DFc–$loxP_p$ after the reaction with Cre. Orange and blue arrows indicate substrates and synaptic complexes, respectively. Image size: 800 × 600 nm. (B) Time-course analysis of the appearance of synaptic complex (cross-shape with bound protein). The number of the DNA frames observed was counted (total of 250–400 DNA frames analyzed for each time point). Error bars represent the standard deviation based on three different imaging experiments. (C) Successive HS-AFM images of a DFc–$loxP_p$–Cre complex which returned back to substrate configuration. Images were obtained at scan rate of 1.0 frame/s. The elapsed time is shown in each image. Image size: 180 × 180 nm. Details are seen in Movie S3.

imaging in combination with a DNA origami nanoscaffold, individual recombination reactions between *loxP* sites mediated by Cre were monitored. In addition, statistical imaging analyses yielded information about the cleavage biases in the step of HJ resolution. The obtained results provide significant insights into the role of substrate DNA topology in the reaction progress and determination of the cleavage order. These results may shed further light on the fundamental mechanisms of Cre–*loxP* recombination.

Requirement of Antiparallel *loxP* sites in Synaptic Complex for the Cre Recombination. Detailed crystallography studies of Cre–*loxP* structures have proposed that the two *loxP* sites are in antiparallel orientation when in the Cre–*loxP* synaptic complex. However, because there are no experimental methods to regulate the orientation of the two DNA strands, the influence of substrate *loxP* site orientation on the synapsis and the subsequent reaction has remained ambiguous. Use of a DNA origami nanoscaffold allowed us to address this issue. Both statistical time-course and individual time-lapse AFM analyses revealed that the *loxP* sites in antiparallel can be converted from the substrates to recombinant products in the DNA frame through the formation of synaptic complexes. By contrast, the sites in parallel did not recombine efficiently even though they were synapsed. This finding supports the idea that an antiparallel orientation of *loxP* sites in the synaptic complex is a prerequisite for the recombination to proceed. We propose that this feature of the reaction may allow one to control the Cre-mediated site-specific recombination by adjusting the relative orientation of the substrate *loxP* sites. If so, this suggests the possibility of using the Cre–*loxP* system as a regulatory tool for DNA manipulations in DNA origami-based nanodevices.

Cre Tetramer Binding to Parallel *loxP* Site-Containing Strands. It is intriguing that the Cre tetramer was seen to form a synaptic complex with two *loxP* sites arranged in parallel in the DFc. Because incorporation of dsDNAs into the DFc was achieved only through the hybridization between their 5′-overhangs and corresponding connectors of the DF, we can assume that the bridged *loxP*-containing DNA strands are rotatable around the helical axis. This rotational motion allows the parallel arrangement of symmetric 13-bp Cre-binding sequences in *loxP* to turn into the antiparallel arrangement (Figure S15). We note that the asymmetric 8-bp spacer sequence remains in parallel even if the strands are rotatable. Consequently, Cre can form a tetramer even though two *loxP* sites are arranged in parallel in the DF but is incapable of progressing the recombination. Although recent single-molecule experiments have indicated the existence of a nonproductive complex in certain populations,[15,16] the details have not been clear. The Cre–*loxP* complex in the above-mentioned situation provides a possible explanation of the reported nonproductive complexes.

Regulation of Cleavage Preference in the DNA Origami Nanoscaffold. By using antiparallel HJ intermediate in DFc as a starting substrate, we analyzed the order of cleavage reaction with wild-type Cre and unmodified *loxP* sites. As suggested by biochemical assays,[26] Cre preferentially resolved the HJ substrates by A↓T cleavage. However, intriguingly, this rule was not followed when HJ intermediates were tethered in DFp, in which the angles between the DNA arms were kept at ∼120° or ∼60°, which demonstrated preferential cleavage of $loxP_{ap}$HJ-b′ at the G↓C sites (Figure 6D). In addition, $loxP_{ap}$HJ-a′ was more strongly biased to A↓T cleavage compared with DFc-incorporated $loxP_{ap}$HJ-a and $loxP_{ap}$HJ-b (Figures 5C,D and 6C). These results suggest that the resolution toward products is biased by the topological states of the HJ intermediates. We note that crystallographic studies of Cre–DNA complexes have shown asymmetric bends in the spacer regions.[29] Thus, it is thought that the catalytic preferences of Cre reflect a balance between the sequence-derived flexibility of the spacer DNA and the interaction of the protein with its substrate. Our results provide evidence that the bending state of the intermediates is a key factor for the bias. It is also noteworthy that the reaction products from DF_p-incorporated junction can be imposed in two different constraint states, i.e. relatively straight state (Type I′) or bent state (Type II′). Considering the preferential accumulation of the Type I′ product, the reaction perhaps proceeds to more energetically favorable constraint state of the product strands. The desired products of the reaction can be efficiently obtained by regulating the topology or geometric constraints of the HJ intermediate.

AFM Imaging Assay Combined with DNA Origami Nanoscaffold. The formation of synaptic DNA–protein complexes is a key step in various genetic processes such as recombination, genome integration, excision, and inversion of specific DNA regions. As in the case of Cre, organization of two DNA regions within a protein–DNA complex would be fundamental for the proteins, which require formation of synaptic complexes to exert their functions. We believe that the methods presented, which are based on the DNA origami

dx.doi.org/10.1021/ja408656y | J. Am. Chem. Soc. 2014, 136, 211–218

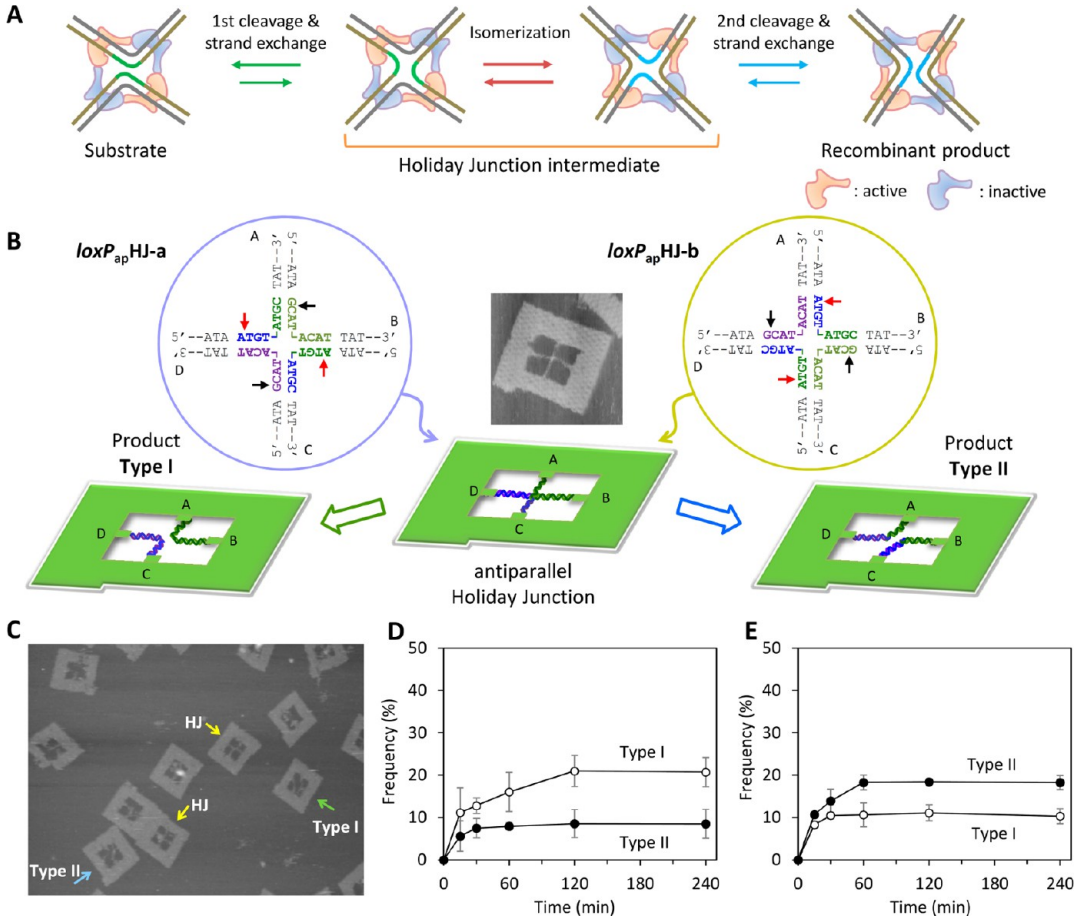

Figure 5. Resolution of *loxP*-derived HJ intermediates tethered in DFc. (A) Schematic of the recombination pathway. The active and inactive proteins are represented by orange and blue, respectively. (B) Schematic of incorporation of HJ structures into the DFc and possible configurations of the resolved DNA strands in the DFc. AFM image shows a DFc carrying *loxP*$_{ap}$HJ-a. Image size: 180 × 180 nm. Two different connection patterns of a *loxP*-derived HJ (*loxP*$_{ap}$HJ-a or *loxP*$_{ap}$HJ-b) were examined. Positions of G↓C cleavage (black arrows) and A↓T cleavage (red arrows) are indicated in the 14-bp core of the two HJ sequences. The 8-bp spacer in *loxP* is highlighted in red. (C) Representative AFM image of DFc−*loxP*$_{ap}$HJ-a after the reaction with Cre. Yellow, green, and blue arrows indicate HJ, type I, and type II structures, respectively. Image size: 800 × 600 nm. (D, E) Time-course analysis of the appearance of type I and type II configurations. The number of each type of DNA frames observed was counted (total of 250−400 DNA frames analyzed for each time point). Error bars represent the standard deviation based on three different imaging experiments.

nanoscaffold and AFM imaging, provide a new platform for the analysis of the interactions between those proteins and DNA. We note that various topological states of HJ structures can be constructed in the nanoscaffold, paving the way for the single-molecule analysis of the junction-binding enzymes involved in junction-resolving reactions and branch migration. We suggest that further extension of our approach might shed new light on the mechanisms underlying communication between two DNA sites and subsequent enzymatic reaction processes.

MATERIALS AND METHODS

Design of DNA Frame Structures. The DNA frame with two pairs of perpendicular connectors (DFc) was designed using caDNAno software. The sequence of the M13mp18 was used, and the staple strands (most of them are 32 mer) were assigned for the formation of the designed DFc. The DFc has the small square at the left bottom corner for the identification of the orientation of the frame (orientation marker). The sequence and positions of the staple strands are listed in the Supporting Information. The DNA frame with two pairs of parallel connectors (DFp) was designed and constructed as previously reported.[17]

DNA Frame Formation. The DNA frames (DFc or DFp) were assembled in a 20 μL solution containing 10 nM of M13mp18 single-stranded DNA (New England BioLabs, Ipswich, MA), 100 nM of staple strands (226 strands), 20 mM Tris-HCl (pH 7.6), 1 mM EDTA, and 10 mM $MgCl_2$. When fixation of the sample is required, 20 mM HEPES-KOH (pH 7.6) was used instead of 20 mM Tris-HCl (pH 7.6). The mixture was annealed from 85 to 15 °C at a rate of −1.0 °C/min. The preassembled two different duplexes or HJ structures were subsequently incorporated into the DNA frame by annealing the mixture from 40 to 15 °C at a rate of −0.5 °C/min using thermal cycler. The sample was purified by gel-filtration chromatography (GE sephacryl-400, GE Healthcare Japan, Tokyo, Japan). The sequences for incorporated duplex strands and HJs are listed in the Supporting Information.

Time-Lapse AFM Imaging of Individual Reaction. The recombination reactions were imaged as follows: 20 nM of Cre (New England BioLabs) was preincubated with 8 nM of the DNA frame carrying two dsDNAs at 37 °C for 5 min in a Tris-buffer [20 mM Tris-HCl (pH 7.6), 1 mM EDTA, 33 mM NaCl, and 10 mM $MgCl_2$]. After the incubation, 2 μL of the sample was immediately deposited onto a freshly cleaved mica disc. After 30 s incubation, the sample was rinsed 10 μL of the Tris-buffer and imaged in the same buffer.

Statistic Time-Course Analysis by AFM. Cleavage reactions were performed by mixing 50 nM of Cre and 8 nM of the DNA frame carrying two dsDNAs in a HEPES-buffer [20 mM HEPES-NaOH (pH 7.6), 1 mM EDTA, 33 mM NaCl, and 10 mM $MgCl_2$]. Aliquots were taken at appropriate time intervals and fixed by mixing 1:1 (v/v) with

dx.doi.org/10.1021/ja408656y | J. Am. Chem. Soc. 2014, 136, 211−218

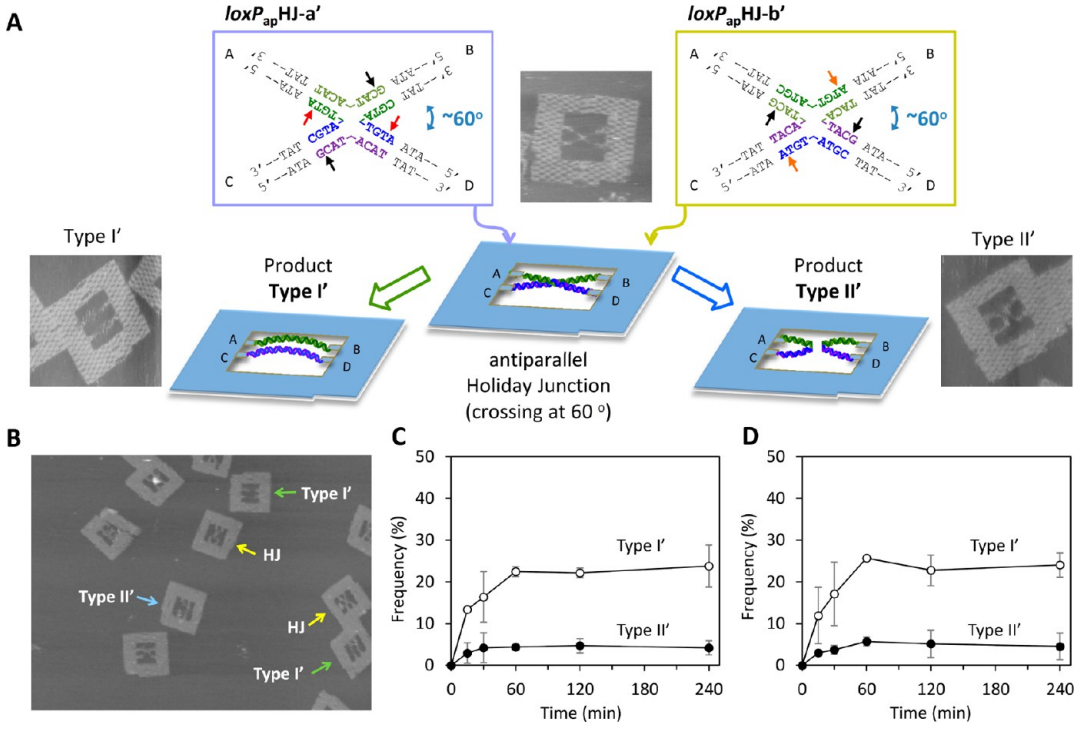

Figure 6. Resolution of *loxP*-derived HJ intermediates tethered in DFp. (A) Schematic of incorporation of HJ structures into a DFp and possible configurations of the resolved DNA strands in the DFp. Each configuration was illustrated together with corresponding AFM image. Image size: 180 × 180 nm. Two different connection patterns of the *loxP*-derived HJ (*loxP*$_{ap}$HJ-a′ or *loxP*$_{ap}$HJ-b′) were examined. Positions of G↓C cleavage (black arrows) and A↓T cleavage (red arrows) are indicated in the 14-bp core of the two HJ sequences. The 8-bp spacer in *loxP* is highlighted in red. (B) Representative AFM image of DFp-*loxP*$_{ap}$HJ-a′ after the reaction with Cre. Yellow, green, and blue arrows indicate HJ, Type I′, and Type II′ structures, respectively. Image size: 800 × 600 nm. (C, D) Time-course analysis of the appearance of Type I′ and II′ configurations. The number of each type of DNA frames observed was counted (total of 250−350 DNA frames analyzed for each time point). Error bars represent the standard deviation based on three different imaging experiments.

0.04% glutaraldehyde in the HEPES-buffer. Following 15 min incubation at 25 °C, the fixation reaction was terminated by a 2-fold dilution into the Tris-buffer [20 mM Tris-HCl (pH 7.6), 1 mM EDTA, 33 mM NaCl, and 10 mM $MgCl_2$]. Excess volume of unbound proteins were removed by gel-filtration chromatography (GE sephacryl-400, GE Healthcare Japan, Tokyo, Japan). For AFM imaging, 2 μL of the sample was deposited onto a freshly cleaved mica disc. After 30 s incubation, the sample was rinsed 10 μL of the buffer and imaged in the Tris-buffer. The number of each type of structures observed in individual scan area (800 × 600 nm or 600 × 480 nm) was counted and summed up (total of 48−64 scans areas examined for each time point). Frequency increases in the appearance of distinct structures were calculated by subtracting initial populations (at 0 min; without protein) from those in each time point.

AFM Imaging. Imaging was performed using a high-speed AFM (Nano Live Vision, RIBM, Tsukuba, Japan). The sample was imaged in the imaging buffer solution at ambient temperature using small cantilevers with dimensions ($L \times W \times H$) of 10 × 2 × 0.1 μm (BL-AC10EGS, Olympus Corporation, Tokyo, Japan). These cantilevers have a spring constant of 0.1−0.2 N/m with a resonant frequency of 400−1000 kHz in water. A sharp probe was deposited on each cantilevers using electron beam deposition by Nanotools (Munich, Germany). The 320 × 240 pixel images were obtained at a scan rate of 0.2−1.0 fps.

■ ASSOCIATED CONTENT

Supporting Information

Additional AFM images, HS-AFM movies, and DNA sequences of DNA substrates and origami scaffold. This material is available free of charge via the Internet at http://pubs.acs.org.

■ AUTHOR INFORMATION

Corresponding Authors

endo@kuchem.kyoto-u.ac.jp

hs@kuchem.kyoto-u.ac.jp

Notes

The authors declare no competing financial interest.

■ ACKNOWLEDGMENTS

We thank the CREST grant from the Japan Science and Technology Corporation (JST) and JSPS KAKENHI (grant nos. 24310097, 24104002, 25253004). Financial supports from The Mitsubishi Foundation and The Asahi Glass Foundation to M.E. are also acknowledged.

■ REFERENCES

(1) Hoess, R. H.; Ziese, M.; Sternberg, N. *Proc. Natl. Acad. Sci. U.S.A.* **1982**, *79*, 3398.

(2) Hoess, R. H.; Abremski, K. *Proc. Natl. Acad. Sci. U.S.A.* **1984**, *81*, 1026.

(3) Mack, A.; Sauer, B.; Abremski, K.; Hoess, R. *Nucleic Acids Res.* **1992**, *20*, 4451.

(4) Abremski, K.; Hoess, R. *J. Biol. Chem.* **1984**, *259*, 1509.

(5) Adams, D. E.; Bliska, J. B.; Cozzarelli, N. R. *J. Mol. Biol.* **1992**, *226*, 661.

(6) Guo, F.; Gopaul, D. N.; van Duyne, G. D. *Nature* **1997**, *389*, 40.

(7) Stark, W. M.; Boocock, M. R.; Sherratt, D. J. *Trends Genet.* **1992**, *8*, 432.

(8) Sauer, B. *Methods Enzymol.* **1993**, *225*, 890.

(9) Kuhn, R.; Schwenk, F.; Aguet, M.; Rajewsky, K. *Science* **1995**, *269*, 1427.

(10) Le, Y.; Sauer, B. *Methods Mol. Biol.* **2000**, *136*, 477.
(11) Hamilton, D. L.; Abremski, K. *J. Mol. Biol.* **1984**, *178*, 481.
(12) Ghosh, K.; Guo, F.; Van Duyne, G. D. *J. Biol. Chem.* **2007**, *282*, 24004.
(13) Rufer, A.; Neuenschwander, P. F.; Sauer, B. *Anal. Biochem.* **2002**, *308*, 90.
(14) Vetcher, A. A.; Lushnikov, A. Y.; Navarra-Madsen, J.; Scharein, R. G.; Lyubchenko, Y. L.; Darcy, I. K.; Levene, S. D. *J. Mol. Biol.* **2006**, *357*, 1089.
(15) Fan, H. F. *Nucleic Acids Res.* **2012**, *40*, 6208.
(16) Pinkney, J. N.; Zawadzki, P.; Mazuryk, J.; Arciszewska, L. K.; Sherratt, D. J.; Kapanidis, A. N. *Proc. Natl. Acad. Sci. U.S.A.* **2012**, *109*, 20871.
(17) Endo, M.; Katsuda, Y.; Hidaka, K.; Sugiyama, H. *J. Am. Chem. Soc.* **2010**, *132*, 1592.
(18) Endo, M.; Katsuda, Y.; Hidaka, K.; Sugiyama, H. *Angew. Chem., Int. Ed.* **2010**, *49*, 9412.
(19) Sannohe, Y.; Endo, M.; Katsuda, Y.; Hidaka, K.; Sugiyama, H. *J. Am. Chem. Soc.* **2010**, *132*, 16311.
(20) Endo, M.; Yang, Y.; Suzuki, Y.; Hidaka, K.; Sugiyama, H. *Angew. Chem., Int. Ed.* **2012**, *51*, 10518.
(21) Rajendran, A.; Endo, M.; Hidaka, K.; Lan Thao Tran, P.; Mergny, J. L.; Sugiyama, H. *Nucleic Acids Res.* **2013**, *41*, 8738.
(22) Rajendran, A.; Endo, M.; Hidaka, K.; Sugiyama, H. *J. Am. Chem. Soc.* **2013**, *135*, 1117.
(23) Hoess, R.; Wierzbicki, A.; Abremski, K. *Proc. Natl. Acad. Sci. U.S.A.* **1987**, *84*, 6840.
(24) Lee, L.; Sadowski, P. D. *J. Mol. Biol.* **2003**, *326*, 397.
(25) Ghosh, K.; Lau, C. K.; Gupta, K.; Van Duyne, G. D. *Nat. Chem. Biol.* **2005**, *1*, 275.
(26) Lee, L.; Sadowski, P. D. *J. Biol. Chem.* **2001**, *276*, 31092.
(27) Martin, S. S.; Pulido, E.; Chu, V. C.; Lechner, T. S.; Baldwin, E. P. *J. Mol. Biol.* **2002**, *319*, 107.
(28) Ennifar, E.; Meyer, J. E.; Buchholz, F.; Stewart, A. F.; Suck, D. *Nucleic Acids Res.* **2003**, *31*, 5449.
(29) Guo, F.; Gopaul, D. N.; Van Duyne, G. D. *Proc. Natl. Acad. Sci. U.S.A.* **1999**, *96*, 7143.